J. Fluid Mech. (2009), *vol.* 632, *pp.* 5–16.
doi:10.1017/S0022112009007381 Printed in the United Kingdom

Growth and collapse of a vapour bubble in a microtube: the role of thermal effects

CHAO SUN, EDIP CAN, RORY DIJKINK, DETLEF LOHSE AND ANDREA PROSPERETTI

Physics of Fluids Group, Faculty of Science and Technology, University of Twente, The Netherlands

(Received 1 September 2008 and in revised form 4 April 2009)

The growth and collapse of a vapour bubble inside a microtube is studied both experimentally and theoretically. The length of the bubble, and the velocity and acceleration of its interface, are obtained from a high-speed image recording (typically 1.25×10^5 fps) for various energy inputs and two tube diameters. To understand the underlying dynamics of the system, two theoretical models are compared with experiment. A model based on a discontinuous time dependence of the vapour pressure inside the bubble is at variance with the data. It proves necessary to account in greater detail for the time dependence of the vapour pressure. A new model is proposed for this purpose which includes heat transfer in addition to inertia and viscous friction. Both the data and the model show that the vapour pressure decreases with time continuously instead of abruptly. The length, velocity and acceleration from the numerical simulations are found to be in good agreement with experimental data. Both the experiments and simulations clearly indicate that thermal effects play an important role throughout the whole growth and collapse process.

1. Introduction

The dynamics of a free bubble have been studied extensively (see, e.g. Plesset & Prosperetti 1977; Brennen 1995; Brenner, Hilgenfeldt & Lohse 2002) due to their relevance for a wide range of phenomena. The first studies devoted to bubbles in confined geometries were motivated by the development of ink-jet printing technology (Allen, Meyer & Knight 1985; Asai 1989, 1991). This early interest has been subsequently sustained by the rapid development of microfluidics (see, e.g. Mazouchi & Homsy 2000; Ajaev, Homsy & Morris 2002; Ajaev & Homsy 2006). Other applications have focused on the actuation properties of rapidly growing and collapsing bubbles. For example, the high liquid velocity induced by transient bubbles has been used to provide high-Reynolds-number flow in microsystems (Ohl *et al.* 2006). Yuan & Prosperetti (1999) and Ory *et al.* (2000) have studied the dynamics of highly transient vapour bubbles in a tube and have demonstrated a pumping effect (Yin & Prosperetti 2005*a*, *b*; see also Jun & Kim 1996, 1998).

Here we study the growth and collapse of a vapour bubble inside a microtube both experimentally and theoretically. In previous studies (Asai 1989; Yin & Prosperetti 2005*a*, *b*), the vapour bubble was created using a thin-film heater at the tube surface. In the present work, the bubble is generated in the central region of a tube by focusing a laser pulse. The experiments are conducted varying the tube diameter and length

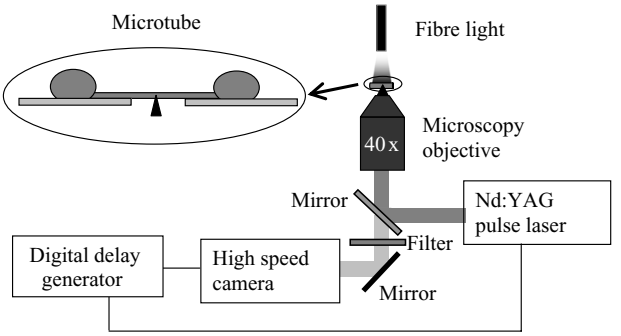

FIGURE 1. A sketch of the experimental setup.

and the laser energy. To increase heat absorption by the liquid, water mixed with dye is used.

The early models (Ory *et al.* 2000; Yin, Prosperetti & Kim 2004; Yin & Prosperetti 2005*a*, *b*) of these processes assumed that the high vapour pressure in the bubble caused by the initial heat pulse persisted only for a very short time and the subsequent dynamics was mostly governed by inertial and viscous effects. We find that these essentially mechanical models are inadequate to describe the observations and develop a new model which incorporates thermal effects.

2. Experimental setup

A sketch of the experimental setup, similar to the one used in the earlier experiments of Zwaan *et al.* (2007), is shown in figure 1. Two glass microtubes were used in the experiments, one with an inner diameter $D = 50\,\mu\text{m}$, outer diameter 80 μm and length $L = 27\,\text{mm}$, the other one with an inner diameter of 24.9 μm, outer diameter 80 μm and length 25 mm. For all experiments the same mixture of water and red food dye was used. The tubes were filled with the liquid, and both ends were covered by large droplets of the same solution (diameter $\sim 5\,\text{mm}$) exposed to the atmosphere. The bubble was created at the midpoint of the microtube by focusing a laser pulse of a wavelength 532 nm (Nd:YAG laser, Solo PIV, New Wave, Fremont, CA, USA) with a time duration of 6 ns by means of a 40× objective. The energy of the laser varied from 27.6 to 49.3 μJ for the $D = 50\,\mu\text{m}$ tube, and from 27.6 to 56.3 μJ for the $D = 24.9\,\mu\text{m}$ tube. For calibrating the energy, an energy meter (Gentec-eo XLE4) was positioned above the tubes. The energy absorbed by the working fluid was calibrated by measuring the difference of the reading of the meter with the empty glass tube and the glass tube filled with the working fluid. For the $D = 50\,\mu\text{m}$ tube, the absorbed energy varied from 6.5 to 11.6 μJ. The energy absorbed by the liquid in the $D = 24.9\,\mu\text{m}$ tube varied from 3.0 to 6.1 μJ.

A filter was used to block the reflected laser light to prevent damage to the camera. The motion of the bubble was recorded by a high-speed camera with a maximum frame rate of 10^6 fps (HPV-1, Shimadzu Corp., Japan). In the experiments, 1.25×10^5 fps proved sufficient. The inter-frame and exposure times are 8 and 4 μs, respectively. The maximum uncertainty of the bubble size due to blurring on a single frame is less than 5 % when the velocity of the interface is maximum. Illumination for the camera was provided by a fibre lamp (Olympus ILP-1) emitting a light spectrum part of which passed through the filter to the camera. A digital delay generator (Model

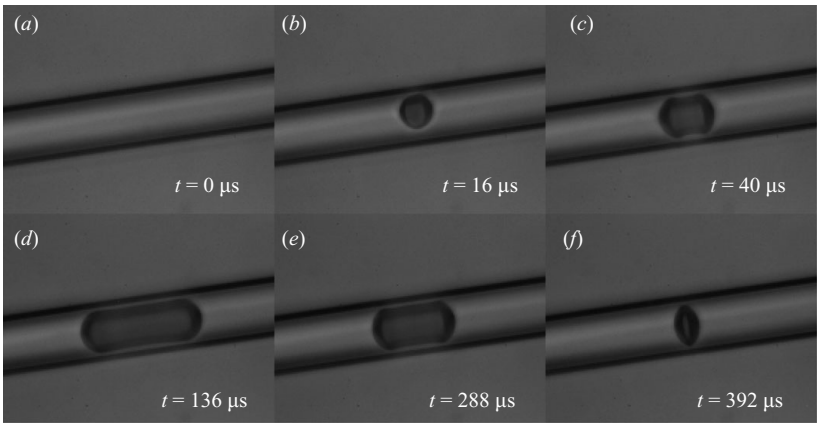

FIGURE 2. Representative frames of the vapour bubble evolution inside the microtube with an inner diameter 50 μm and length 27 mm; the absorbed laser energy is 11.6 μJ.

555, Berkeley Nucleonics Corp., CA, USA) was used to synchronize the camera and the laser.

3. Experimental results

Some representative frames taken during the evolution of the vapour bubble in the larger tube are shown in figure 2. The tube is initially full of liquid as shown in figure 2(*a*). The vapour bubble appears rapidly at the midpoint of the tube after the liquid has absorbed 11.6 μJ from the laser pulse. The bubble is initially a small sphere (figure 2*b*), it expands spherically until it nearly occupies the whole diameter of the tube, after which preferential growth in the axial direction begins (figure 2*c*). The shape of the bubble changes approximately to that of a cylinder occupying the majority of the cross-section of the tube (figure 2*c–e*). A very thin liquid film on the tube wall, as expected from the no-slip condition on a hydrophilic surface, is barely visible in these pictures and with insufficient detail for a quantitative study. The appearance of the bubble during the expansion (figure 2*c*) and collapse (figure 2*e*) is similar except for the final stage (figure 2*f*), where it differs appreciably from its shape at the moment of formation (figure 2*b*). The final shape is oblate and the motion remains very nearly one-dimensional until the very end because surface tension does not have the time to make the interface curved. Thus, the flow retains its approximately one-dimensional nature due to its brief duration (Ory *et al.* 2000), which makes a one-dimensional model a reasonable approximation.

By approximating the bubble as a cylinder, its length L_{bubble} along the axis of the tube and its diameter W can be extracted from the high-speed movies. The volume of the bubble is calculated as $V_{bubble} = \pi W^2 L_{bubble}/4$. The bubble volume in this way involves some error which is only appreciable in the first few frames. The estimated errors for figures 2(*b*), 2(*c*) and 2(*d*) are 25 %, 10 % and 4 %, respectively. Since the system is symmetric with respect to the midpoint of the tube, we only consider half of the bubble. From here on, the bubble length is defined as $X = (1/2)V_{bubble}/(\pi D^2/4)$.

The time evolution of the measured bubble length X for different energy levels in the larger tube is plotted with open symbols in figure 3(*a*). In descending order, the absorbed energy is 11.6, 10.4, 8.2 and 6.5 μJ. The maximum bubble size and its duration increase with increasing energy. The overall trends of the $X(t)$ curves for

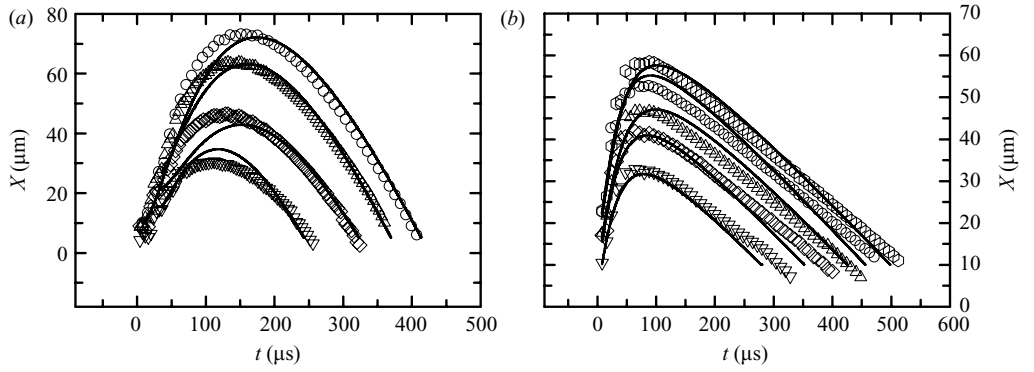

FIGURE 3. Time evolution of the bubble length X for different energy levels (a) in the tube with $D = 50\,\mu\text{m}$; in descending order $E = 11.6$, 10.4, 8, 2 and $6.5\,\mu\text{J}$; (b) in the tube with $D = 24.9\,\mu\text{m}$, for $E = 6.1$, 5.3, 4.8, 3.8 and $3.0\,\mu\text{J}$. The open symbols are the experimental results and the lines are the results of the thermal model. See text for detailed parameters for the model.

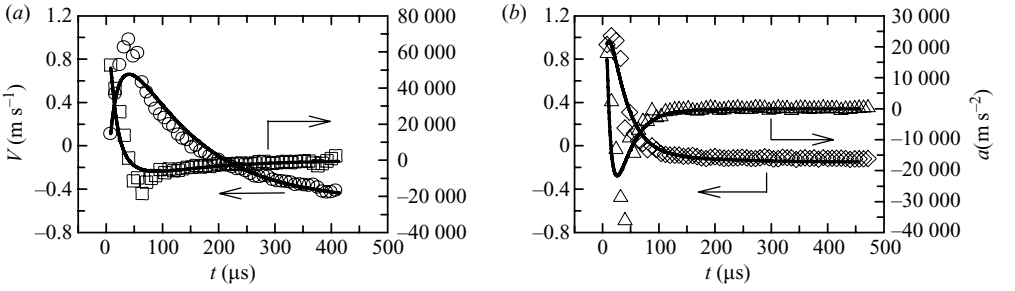

FIGURE 4. Velocity and acceleration of the interface versus time. (a) $D = 50\,\mu\text{m}$ with $E = 11.6\,\mu\text{J}$, and (b) $D = 24.9\,\mu\text{m}$ with $E = 5.3\,\mu\text{J}$. The open symbols are the experimental results and the lines the numerical results given by the thermal model.

different energy levels are quite similar. The vapour bubble expands quickly, and shrinks more slowly after reaching its maximum size.

The contrast between growth and collapse is even sharper with the smaller tube. The bubble length versus time for different energy levels for this case is shown with open symbols in figure 3(b). More experimental runs were available with this tube and each $X(t)$ curve shown is the result of averaging three different experiments under the same nominal conditions. Shot-to-shot reproducibility was good. In descending order, the absorbed energy is 6.1, 5.3, 4.8, 3.8 and $3.0\,\mu\text{J}$. Again, the maximum length and the duration of the bubble increase with increasing energy and the overall trends of the $X(t)$ curves for different energy levels are quite similar. However, the collapse of the bubble in this case proceeds much slower than its expansion. Unlike the larger tube case, the collapse process lasts about 10 times longer than the expansion.

To fit the measured $X(t)$, we used cubic splines from which the velocity and acceleration of the liquid/vapour interface can be extracted. The time dependence of the velocity in the larger tube is shown for $E = 11.6\,\mu\text{J}$ by the circles in figure 4(a). The velocity of the interface increases quickly to a maximum around $1\,\text{m s}^{-1}$ at $t \sim 40\,\mu\text{s}$, and then decreases continuously to a minimum value around $-0.4\,\text{m s}^{-1}$ when the bubble disappears. The time dependence of the velocity in the smaller tube, for $E = 5.3\,\mu\text{J}$, is shown by the open diamonds in figure 4(b). The velocity of the

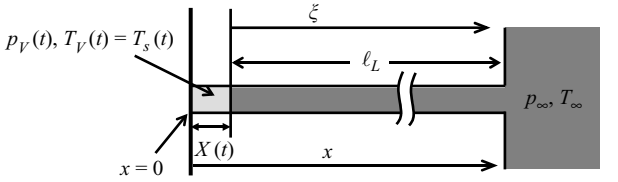

FIGURE 5. Conceptual sketch used in the formulation of the thermal model.

interface increases to around $1\,\mathrm{m\,s^{-1}}$ at $t \sim 16\,\mu\mathrm{s}$ and then decreases continuously. The maximum velocity in the smaller tube is reached earlier than in the larger tube and the collapse velocity ($0.2\,\mathrm{m\,s^{-1}}$) is lower than that in the larger tube ($0.4\,\mathrm{m\,s^{-1}}$). Since the very first instants of the bubble growth were too fast to be recorded, the first data readings that could be taken correspond to a finite velocity.

The acceleration of the interface is also shown in figure 4(*a*). Here the squares are for the larger tube with $E = 11.6\,\mu\mathrm{J}$. The acceleration begins with a huge value around $55\,000\,\mathrm{m\,s^{-2}}$, then immediately becomes negative down to around $-10\,000\,\mathrm{m\,s^{-2}}$, and finally increases again to a very small value. The huge value at the beginning is a remarkable feature which may be potentially useful in microfluidic systems. The acceleration of the interface in the smaller tube, with $E = 5.3\,\mu\mathrm{J}$, is shown by the triangles in figure 4(*b*). It begins with a positive value around $20\,000\,\mathrm{m\,s^{-2}}$, and decreases rapidly to a negative value around $-35\,000\,\mathrm{m\,s^{-2}}$, after which it increases quickly to a very small value. The stronger deceleration for the thinner tube reflects the enhanced viscous forces on the small scale.

We now describe two simple theoretical models which are helpful to shed some light on these observations.

4. Theoretical models

As remarked before, the approximate one-dimensional nature of the bubble evolution suggests the possibility of using a simple one-dimensional model for its behaviour which is sketched in figure 5. Here the left vertical line is the plane of symmetry at the midpoint of the tube which coincides with the centre of the bubble. We are interested in the motion of the right vapour–liquid interface located at $X(t)$. If the pressure at the other end of the liquid column is a constant p_∞, the equation of motion of the liquid column in the tube is, approximately (Yin *et al.* 2004),

$$\ell_L \rho_L \frac{\mathrm{d}^2 X}{\mathrm{d}t^2} = p_V(t) - p_\infty - \mathscr{R}\frac{\mathrm{d}X}{\mathrm{d}t}. \tag{4.1}$$

Here ℓ_L is the length of the liquid column, which we keep constant and equal to half of the tube length given the smallness of the the bubble; p_V is the vapour pressure in the bubble and $\mathscr{R}$ represents on approximation the effect of viscous losses due to the wall. By approximating the flow in the tube as quasi-steady fully developed Poiseuille flow, we model this term as $\mathscr{R} = 32\mu\ell_L/D^2$, in which μ is the liquid viscosity. This approximation is justified if the viscous diffusion length is comparable to, or larger than, the tube radius $D/2$, i.e. $2\sqrt{\nu\tau_b}/D \gtrsim 1$. With a bubble duration $\tau_b \simeq 400\,\mu\mathrm{s}$ and $D = 50\,\mu\mathrm{m}$, this ratio is about 0.8. This value does not fully support the approximation, which will therefore tend to underestimate somewhat the true viscous loss. However the error may be expected to be moderate, which is supported by the results that will be shown later. Since the pressure inside the bubble is essentially uniform there is no

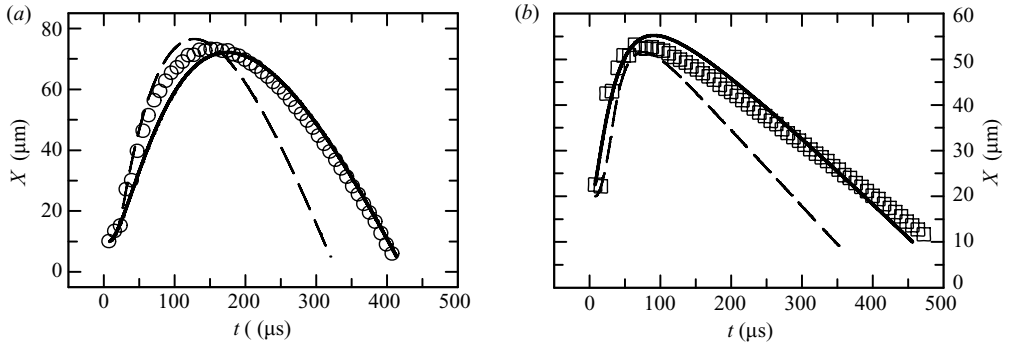

FIGURE 6. Comparison of the bubble length $X(t)$ versus time as measured and predicted by the models for the cases (*a*) $D = 50\,\mu\text{m}$ and (*b*) $D = 24.9\,\mu\text{m}$. The open symbols are the experimental results; the dashed lines are the predictions of the step-function pressure model and the solid lines those of the thermal model.

pressure gradient to drive the flow in the film so that viscous dissipation in it can be neglected.

4.1. *The step-function pressure model*

In the past work (see, e.g. Ory *et al.* 2000) the dynamics of the bubble was modelled including inertia and viscosity but neglecting thermal effects. The pressure inside the bubble was taken equal to the vapour pressure of the liquid at the initial undisturbed temperature, except for a short interval $0 \leqslant t < \Delta t$ during which it was given a large value $p_\infty + \Delta p$. We can now compare the predictions of this model with our data.

This simple model has two free parameters, Δp and the duration of the overpressure Δt. As suggested by the data to be shown later, we take the initial high pressure $p_V = p_\infty + \Delta p = 10^6\,\text{Pa}$ and fit Δt so as to match approximately the observed maximum elongation of the bubbles in figure 3. For the larger tube ($D = 50\,\mu\text{m}$) and $E = 11.6\,\mu\text{J}$ we take $\Delta t = 22\,\mu\text{s}$ while, for the smaller tube ($D = 24.9\,\mu\text{m}$) with $E = 5.3\,\mu\text{J}$, we take $\Delta t = 25\,\mu\text{s}$. For $t > \Delta t$ the pressure inside the bubble falls to $p_V = p_V(25^\circ\text{C}) = 3.2 \times 10^3\,\text{Pa}$. The initial bubble length for both cases was selected from experiment, $X(0) = 10\,\mu\text{m}$ for $D = 50\,\mu\text{m}$ and $X(0) = 20\,\mu\text{m}$ for $D = 24.9\,\mu\text{m}$. The initial velocity for both cases was taken as 0.

The results of this step-function pressure model for the two cases are shown with the dashed lines in figure 6. The open symbols are the experimental data (*a*) $D = 50\,\mu\text{m}$ with $E = 11.6\,\mu\text{J}$ and (*b*) $D = 24.9\,\mu\text{m}$ with $E = 5.3\,\mu\text{J}$. Although in a very general way some aspects of the observed bubble dynamics are reproduced, a major difference between this model and our data lies in the much faster collapse than in the experiment. This aspect cannot be changed by simply playing with the free parameters Δp, Δt and the initial velocity of the interface.

In order to get some insight into the failure of this model, we use the dynamic equation (4.1) in reverse to calculate p_V from the measured velocity and acceleration of the bubble interface. If we assume that the vapour is saturated, we can calculate the vapour temperature $T_S(t)$ from $p_V(t)$ by using the approximate relation

$$p_V = p_{V0} \exp\left[\frac{H_{Latent}}{R_v}\left(\frac{1}{T_0} - \frac{1}{T_S}\right)\right] \tag{4.2}$$

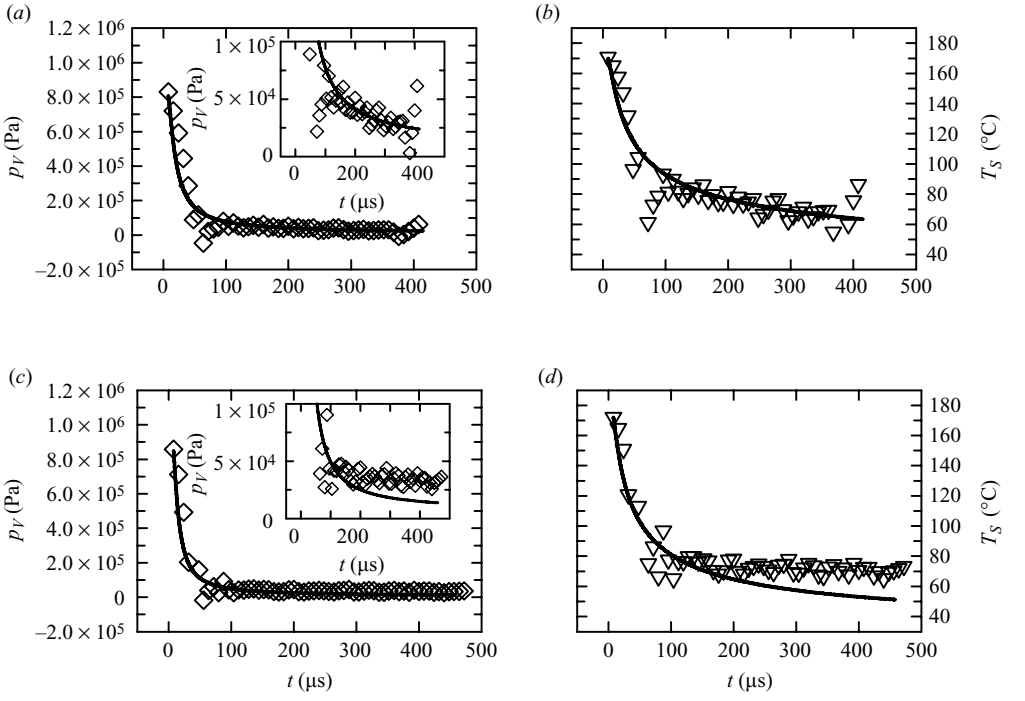

FIGURE 7. Vapour pressure and temperature versus time for (*a*, *b*) the larger tube with $E = 11.6\,\mu\text{J}$, and (*c*, *d*) the smaller tube with $E = 5.3\,\mu\text{J}$. The open symbols are experimental results, the lines the thermal model predictions. The insert in (*a*) and (*c*) shows the vapour pressure versus time on an enlarged vertical scale.

deduced from the Clausius–Clapeyron equation assuming a constant latent heat H_{Latent}; this approximation is legitimate over the limited temperature range of our experiment. In this equation R_v is the universal gas constant divided by the vapour mass; we take $p_{V0} = 10^5$ Pa and $T_0 = 100°\text{C}$.

For $D = 50\,\mu\text{m}$ with $E = 11.6\,\mu\text{J}$, the results of these calculations are shown with open diamonds in figures 7(*a*) and 7(*b*). The pressure starts at around 8 atm, which leads to the huge acceleration of the liquid column. The insert in figure 7(*a*) is the vapour pressure versus time on an enlarged vertical scale, which clearly shows that the pressure decreases with time continuously instead of reaching a constant value. The corresponding vapour temperature is shown by the open triangles in figure 7(*b*). The temperature starts at 170°C, and decreases continuously with time. A very surprising result is that at the finial stage the temperature is still ~60°C instead of the undisturbed liquid temperature ~25°C. The similar trends of the vapour pressure and temperature in the smaller tube with $E = 5.3\,\mu\text{J}$ are shown by open symbols in figures 7(*c*) and 7(*d*).

This analysis shows that the previous model fails because it replaces the actual slow pressure fall by an abrupt decrease.

4.2. *The thermal model*

It is interesting to explore to what extent these data can be reproduced by complementing the mechanical model of (4.1) with a thermal model. For this purpose we write an energy balance for the vapour in the following form (see, e.g. Yang &

Prosperetti 2008):

$$H_{Latent}\frac{\mathrm{d}}{\mathrm{d}t}(\rho_V X) = k\frac{\partial T}{\partial x}\bigg|_{x=X} - \rho_V c_s X\frac{\mathrm{d}T_S}{\mathrm{d}t}. \tag{4.3}$$

The left-hand side of this equation is the latent heat associated with the vapour generation or condensation. The first term on the right-hand side, in which k is the thermal conductivity of the liquid, is the energy conducted to the vapour space from the liquid column. The last term, in which c_s is the specific heat along the saturation curve and $T_S(t) = T(X(t), t)$ is the temperature at the liquid surface, accounts for the energy necessary to maintain the vapour at saturation conditions; c_s is given by $c_s = c_{pV} - H_{Latent}/T_S$ in which the c_{pV} is vapour specific heat (Landau & Lifshitz 1980).

In formulating the energy balance (4.3) we have assumed that the vapour is in spatially uniform conditions and that it exchanges energy by conduction with the liquid column but not with the tube wall. We will return to this point later.

The temperature change of the liquid column is controlled by the advection–diffusion equation

$$\rho_L c_p\left[\frac{\partial T}{\partial t} + \mathbf{u}\cdot\nabla T\right] = k\nabla^2 T, \tag{4.4}$$

where c_p is the liquid specific heat. The thermal penetration length over the duration of the entire process is of the order of 5 μm, which is much less than the tube radius. Furthermore, the initial energy density may be expected to be reasonably uniform radially over the heated liquid volume and the transverse velocities are very small. For this reason, the only significant temperature gradient may be expected to be near the bubble surface so that the equation can be simplified to

$$\rho_L c_p\left[\frac{\partial T}{\partial t} + u\frac{\partial T}{\partial x}\right] = k\frac{\partial^2 T}{\partial x^2}. \tag{4.5}$$

We change the frame of reference to the moving interface by making the coordinate transformation $\xi = x - X(t)$; the final form of the equation is then

$$\rho_L c_p\frac{\partial T}{\partial t} = k\frac{\partial^2 T}{\partial \xi^2}. \tag{4.6}$$

This equation must be solved subject to the boundary conditions

$$T(\xi = 0, t) = T_S(t); \qquad T(\xi = \ell_L, t) = T_\infty. \tag{4.7}$$

In order to solve the liquid diffusion equation we also need to provide the initial temperature profile along the liquid column. This is a matter of considerable uncertainty because we do not have sufficient information on the spatial distribution of the absorbed laser energy. Furthermore, a one-dimensional model cannot capture the detailed three-dimensional character of the initial temperature distribution. Very close to the instant of bubble nucleation, we can envisage a small vapour nucleus surrounded by a hot liquid layer which thins as the vapour expands. By the time the bubble has grown to occupy the cross-section of the tube and the one-dimensional approximation becomes applicable, this layer will be adjacent to the bubble surface on the faces of the two liquid columns which bound it. On this basis, we postulate an initial temperature distribution given by

$$T(\xi) = T_\infty + (T_S(t_0) - T_\infty)\exp[-(\xi/2\delta)^2], \tag{4.8}$$

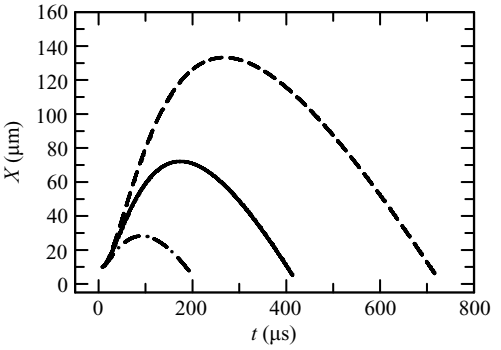

FIGURE 8. Calculated $X(t)$ curves for the thermal model with different values of the parameter δ for the larger tube with the same initial conditions as for $E = 11.6\,\mu\text{J}$; in descending order δ is 4.5, 2.9 and 1.5 μm. The middle line with $\delta = 2.9\,\mu\text{m}$ is the best fit to the experimental data shown in figure 3 and 6.

where $T_S(t_0)$ is the initial vapour temperature and δ is the thickness of the thermal layer surrounding the vapour space. This quantity may be expected to be of the order of the laser beam width and we will use it as a fitting parameter.

We start the integration attributing to the bubble the measured length and velocity at the first instant t_0 at which the movie record shows an effectively one-dimensional bubble near the beginning of each experiment. For the larger tube with $E = 11.6\,\mu\text{J}$, we take the data recorded $t_0 = 8\,\mu\text{s}$ after the laser triggering: initial bubble size $X(t_0) = 10\,\mu\text{m}$, initial velocity $V(t_0) = 0.11\,\text{m s}^{-1}$ and initial vapour temperature $T_S(t_0) = 170^\circ\text{C}$; the initial vapour pressure is calculated from the initial vapour temperature according to (4.2) and is $8.07 \times 10^5\,\text{Pa}$. Furthermore, ℓ_L is 13.5 mm, $p_\infty = 10^5\,\text{Pa}$, $T_\infty = 25^\circ\text{C}$. By choosing the parameter $\delta = 2.9\,\mu\text{m}$ we find the bubble-length versus time shown by the solid line in figure 6(*a*). The time dependence of the bubble size agrees well with experimental data (open circles). The velocity and acceleration of the interface, shown by the solid lines in figure 4(*a*), also agree well with experiment.

The vapour pressure and temperature versus time are shown by the solid lines in figure 7(*a*, *b*). Both predictions are seen to be consistent with the experiment. In particular, the model captures well the continuous decrease of these quantities. It is remarkable also that the final bubble temperature, $\sim 60^\circ\text{C}$, is reproduced by the model.

The actual heat exchange between the bubble and its surroundings is a complex problem for which too little information is available to permit the formulation of a faithful model. The thermal diffusion length over a time of 100 μs is about 4 μm, which is comparable with the thickness of the liquid film deposited on the tube wall, expected to be of the order of micrometres. This liquid layer is probably formed from the liquid heated by the laser pulse and therefore will have some initial energy content. It is therefore not clear whether the tube wall, which should be cold as it will not have absorbed energy from the laser, plays a role in the thermal exchange. In view of all these uncertainties, the one-dimensional thermal model used before may perhaps best be seen as a phenomenological model which appears nevertheless able to capture at least a good part of the relevant physics. The importance of heat diffusion is brought into evidence by the sensitivity of the model to the value of the parameter δ. This point is illustrated in figure 8 which shows the bubble length versus time as obtained with $\delta = 1.5$, 2.9 and 4.5 μm.

D (μm)	E (μJ)	$X(t_0)$ (μm)	$V(t_0)$ (m s^{-1})	$T_S(t_0)$ (°C)	δ (μm)
50	11.6	10.0	0.11	170.0	2.9
	10.4	26.7	0.42	134.7	3.1
	8.2	21.0	0.11	135.7	3.6
	6.5	15.5	0.33	141.3	1.9
24.9	6.1	21.9	0.77	179.4	1.9
	5.3	22.5	0.94	172.0	1.8
	4.8	16.9	0.67	172.7	2.2
	3.8	15.7	0.77	163.2	2.1
	3.0	10.1	0.80	151.2	2.4

TABLE 1. The initial conditions and the respective fitting parameter δ of the thermal model for different energy levels.

The results of the model for the other cases of figure 3(a) are shown by the lines in the same figure. The initial conditions used in each case together with the corresponding value of δ for the larger tube with different energy levels are listed in table 1. At low laser energy it takes a few frames for the bubble to acquire a one-dimensional character and therefore t_0 is somewhat greater. The parameter δ does not change too much except for the lowest energy level. The solid lines in figure 3(a) are the calculated bubble length versus time. A reasonably good agreement is apparent for each energy level. Only at the lower value of the energy does the model start to show some noticeable discrepancy with experiment, presumably because the one-dimensional approximation becomes invalid.

As a typical example for the smaller tube we consider the case with $E = 5.3\,\mu\text{J}$, again taking as the initial conditions the data: $t_0 = 8\,\mu\text{s}$, initial velocity $V(t_0) = 0.94\,\text{m s}^{-1}$, initial bubble size $X(t_0) = 22.5\,\mu\text{m}$, initial vapour temperature $T_S(t_0) = 172.0^\circ\text{C}$ and initial vapour pressure $p_V(t_0) = 8.48 \times 10^5\,\text{Pa}$. Furthermore, ℓ_L is 12.5 mm with p_∞ and T_∞ as before. A reasonable fit to the data is obtained by taking $\delta = 1.8\,\mu\text{m}$. The bubble length versus time calculated from the thermal model is shown by the solid line in figure 6(b). The bubble size versus time again agrees very well with experiment (open squares). The velocity and acceleration of the interface are shown by the solid lines in figure 4(b) and they are both seen to be consistent with experiment. The vapour pressure and temperature versus time in this case are shown by the solid lines in figures 7(c) and 7(d). Although in this case the predictions are not in as good agreement with experiment as for the larger tube, they are nevertheless consistent with observation. It is likely that a significant factor in the difference between model and data is a result of an inaccurate account of viscous effects which play a great role in the smaller tube.

The performance of the model for the other experiments in figure 3(b) is shown by the solid lines in the same figure. The initial conditions and the respective values of δ are listed in table 4.2. The δ-values for different energy levels are quite close, ranging between 1.8 and 2.4 μm. The comparison between the experiments (open symbols) and the calculations shows a very good agreement for all energy levels.

4.3. *Energy partition*

The present model contains both mechanical and thermal aspects and it is interesting to examine how the energy is apportioned among the different components. Let us consider the larger tube $D = 50\,\mu\text{m}$ with an absorbed energy $E = 11.6\,\mu\text{J}$. From figure 4 the maximum velocity is $0.98\,\text{m s}^{-1}$; the corresponding kinetic energy is

$2((1/2)\rho_L S\ell_L \dot{X}^2) \simeq 0.025\,\mu\text{J}$, where $S = \pi D^2/4$ is the tube cross-section and the factor of 2 accounts for both liquid columns. The instantaneous viscous energy dissipated is $2\mathscr{R}S\dot{X}^2\Delta t$, and $2\mathscr{R}S\dot{X}^2$ evaluated at the maximum velocity is $576\,\mu\text{J s}^{-1}$. No matter what value of Δt is selected, this energy term is negligible. If we take $\Delta t = 100\,\mu\text{s}$, $2\mathscr{R}S\dot{X}^2\Delta t = 0.058\,\mu\text{J}$. Both these mechanical energies are much smaller than the laser energy absorbed by the liquid.

The total latent heat necessary to keep the bubble filled with saturated vapour at the point of its maximum volume is $2S\rho_V H_{latent} X_{max}$. At maximum expansion $T_S = 79°\text{C}$, $\rho_V = 0.29\ \text{kg m}^{-3}$, $X_{max} = 72\,\mu\text{m}$ so that $2S\rho_V H_{latent} X_{max} = 0.18\,\mu\text{J}$, which is also much smaller than the $11.6\,\mu\text{J}$ absorbed by the liquid. Where is the remainder of the energy? The answer is that most of the laser energy has gone into heating up the liquid. The energy required to generate the temperature distribution (4.8) is

$$2\int_0^{\ell_L} (T_S(t_0) - T_\infty)\exp[-(\xi/2\delta)^2]c_p\rho S\,\mathrm{d}\xi \tag{4.9}$$

Evaluating this integral using $\delta = 2.9\,\mu\text{m}$, $T_S(t_0) = 170°\text{C}$, we find $\sim 11.7\,\mu\text{J}$, which is quite close to the laser energy input.

5. Conclusions

The dynamics of a laser-generated vapour bubble in microtubes with different diameters has been studied experimentally and theoretically. A pure inertia-driven model, neglecting thermal effects, failed to capture quantitatively the growth and collapse of the bubble. A new model was developed by considering heat transfer in addition to inertia and viscosity. This model has proved to be capable of reproducing the observed behaviour of the bubble. It is concluded that thermal effects play an essential role during the whole process of growth and collapse.

We thank J. Sijl, R. Stevens, J. Snoeijer and C. D. Ohl for stimulating discussions, this work was supported by STW, VIDI & NWO. AP expresses his appreciation to Mr Ran Yaron of ART (Boulder CO) who stimulated some ideas contributed to this work.

REFERENCES

Ajaev, V. S. & Homsy, G. M. 2006 Modeling shapes and dynamics of confined bubbles. *Annu. Rev. Fluid Mech.* **38**, 277–307.

Ajaev, V. S., Homsy, G. M. & Morris, S. J. S. 2002 Dynamic response of geometrically constrained vapour bubbles. *J. Colloid Interface Sci.* **254**, 346–354.

Allen, R. R., Meyer, J. D. & Knight, W. R. 1985 Thermodynamics and hydrodynamics of thermal ink jets. *Hewlett-Packard J.* **36**, 21–27.

Asai, A. 1989 Application of the nucleation theory to the design of bubble jet printers. *Jpn. J. Appl. Phys.* **28**, 909–915.

Asai, A. 1991 Bubble dynamics in boiling under high heat flux pulse heating. *J. Heat Transfer* **113**, 973–979.

Brennen, C. E. 1995 *Cavitation and Bubble Dynamics*. Oxford University Press.

Brenner, M. P., Hilgenfeldt, S. & Lohse, D. 2002 Single-bubble sonoluminescence. *Rev. Mod. Phys.* **74**, 425–484.

Jun, T. K. & Kim, C. J. 1996 Microscale pumping with traversing bubbles in microchannels. In *Solid-State Sensor and Actuator Workshop*, Hilton Head Island, pp. 144–147.

Jun, T. K. & Kim, C. J. 1998 Valveless pumping using traversing vapour bubbles in microchannels. *J. Appl. Phys.* **83**, 5658–5664.

Landau, L. D. & Lifshitz, E. M. 1980 *Statistical Physics*. Pergamon Press.

Mazouchi, A. & Homsy, G. M. 2000 Thermocapillary migration of long bubbles in cylindrical capillary tubes. *Phys. Fluids* **12**, 542–549.

Ohl, C. D., Arora, M., Dijkink, R., Janve, V. & Lohse, D. 2006 Surface cleaning from laser-induced cavitation bubbles. *Appl. Phys. Lett.* **89**, 074102.

Ory, E., Yuan, H., Prosperetti, A., Popinet, S. & Zaleski, S. 2000 Growth and collapse of a vapour bubble in a narrow tube. *Phys. Fluids* **12** (6), 1268–1277.

Plesset, M. S. & Prosperetti, A. 1977 Bubble dynamics and cavitation. *Annu. Rev. Fluid Mech.* **9**, 145–185.

Yang, B. & Prosperetti, A. 2008 Vapour bubble collapse in isothermal and non-isothermal liquids. *J. Fluid Mech.* **601**, 253–279.

Yin, Z. & Prosperetti, A. 2005*a* 'blinking bubble' micropump with microfabricated heaters. *J. Micromech. Microengng* **15**, 1683–1691.

Yin, Z. & Prosperetti, A. 2005*b* A microfluidic 'blinking bubble' pump. *J. Micromech. Microengng* **15**, 1–9.

Yin, Z., Prosperetti, A. & Kim, J. 2004 Bubble growth on an impulsively powered microheater. *Intl J. Heat Mass Transfer* **47**, 1053–1067.

Yuan, H. & Prosperetti, A. 1999 The pumping effect of growting and collapsing bubbles in a tube. *J. Micromech. Microengng* **9**, 402–413.

Zwaan, E., Le-Gac, S., Tsuji, K. & Ohl, C. D. 2007 Controlled cavitation in microfluidic systems. *Phys. Rev. Lett.* **98**, 254501.